RSC Advances

PAPER

View Article Online
View Journal | View Issue

Cite this: *RSC Adv.*, 2015, **5**, 62543

Structural evolution of $(Au_2S)_n$ ($n = 1–8$) clusters from first principles global optimization†

Yiqun Feng and Longjiu Cheng*

We explore the structural evolution of $(Au_2S)_n$ ($n = 1–8$) clusters using a first principles global minimization technique, namely, a genetic algorithm from density functional theory geometry optimization (GA-DFT). The growth sequence and pattern for n from 1 to 8 are analyzed from the perspective of geometric shell formation. The average binding energy, HOMO–LUMO energy gaps, vertical electron affinity, and vertical ionization potential are examined as a function of the cluster size. The global minimum structures are planar at $n = 1–3$, three-dimensional at $n = 4–8$. The formation of these structures are attributed to the high stability of S–Au–S structural unit and particularly the Au_3S_3 and Au_4S_4 rings. Chemical bonding analysis reveals that the three-dimensional clusters ($n = 4–8$) can be viewed as $[Au_{2n-x}S_n]^{x-}\cdot xAu^+$ in electronic structure. The Au^+ cations are not involved in any S–Au covalent bond, however, are attracted by only Au···Au aurophilic interactions. Direct evidence for the Au···Au aurophilicity are given by a noncovalent interaction index analysis. Such Au···Au aurophilic interactions play an important role in the stability of $(Au_2S)_n$ clusters.

Received 7th April 2015
Accepted 13th July 2015

DOI: 10.1039/c5ra06137g

www.rsc.org/advances

Introduction

Gold exhibits many unique properties among the coinage metals because of the strong relativistic effects.[1] Ligand-protected gold nanoparticles (AuNP) have attracted much attention since the discovery of unexpected physical and chemical properties that can be exploited for a variety of applications, ranging from nanocatalysis, medicine, and materials science.[2–6]

Bare gold clusters[7–11] and thiolate-protected gold (Au–SR) clusters[12–15] have been well studied in the past few years and they show distinctive structures, interesting motivated in part by understanding the Au–S interactions and Au···Au contacts which are important in thiol-passivated gold nanoparticles.[8,16,17] Hakkinen and co-workers[13] proposed a superatom model that Au–SR clusters can be understood with the magic numbers of free valence electrons described as the spherical jellium model. Based on the superatom model, the stability and chemical nature of Au–SR clusters has been successful explaining such as $Au_{25}(SR)_{18}^-$ cluster[18,19] and $Au_{102}(SR)_{44}$ cluster.[20] Later, Cheng and Yang proposed a super valence bond model and superatom networks to explain the stability of non-spherical shells of metal clusters,[21,22] such as $Au_{38}(SR)_{24}$.[23,24]

However, for experimental produced Au–SR clusters, the gold-to-thiolate ratio is usually greater than 1 : 1. The low-lying structures of $(AuSR)_n$ ($n = 6–12$), with an exactly 1 : 1 gold-to-thiolate ratio, were studied by Zeng and co-workers[14] using density functional theory (DFT) method. The global minimum double helical structure has a relatively smaller mean Au–Au distance and Au–S–Au angle that is an important indicator of strong Au···Au interaction to characterize the stability of gold-thiolate.

Sulfur-doped gold clusters (Au_xS_y) have also received much attention in recent years. The covalent bond between gold and sulfur and Au···Au interactions are paramount importance in stabilizing the nanostructures. Recently, Pei *et al.*[25] reported several hollow or core-centered polyhedral structures for many gold–sulfide cluster anions ($Au_mS_n^-$). The robustness of the polyhedral structures can be attributed to the high stability of S–Au–S and then to the stable triangular or square faces structural unit (Au_3S_3 or Au_4S_4). However, the gold-to-sulfur ratio is usually 3 : 2 in hollow polyhedral structures. For sulfur-doped gold clusters, the gold-to-sulfur ratio is usually non-stoichiometric. Several researches about sulfur-doped gold clusters with 2 : 1 ratio rule of Au/S at very small sizes were reported several years ago.[26] Other intriguing structures previously found were Cu_2Se and $(Cu_2Se)_n$ clusters.[27,28]

Several M_2S (M = Cu, Ag and Au) nanoparticles[29–31] were synthesized. The Cu_2S and Ag_2S nanoparticles are perfect nanocrystals showing clear hexagonal or cubic lattices.[29,30] However, the structures of Au_2S nanoparticles are very different from those of Cu_2S and Ag_2S nanoparticles, which show cross-sheet-like or plate-like superstructures. The unique structures of Au_2S nanoparticles may due to the strong aurophilic interaction as a consequence of relativistic effects, which plays an important role in the stability of gold clusters.[32,33] It is still little

Department of Chemistry, Anhui University, Hefei, Anhui, 230601, China. E-mail: clj@ustc.edu

† Electronic supplementary information (ESI) available: AdNDP localized bonding patterns of $(Au_2S)_n$ ($n = 5–8$) and atomic coordinates (in Å) of the global minimum structures. See DOI: 10.1039/c5ra06137g

known about the geometric and electronic properties of small stoichiometric $(Au_2S)_n$ clusters, which may also show very unique properties due to the aurophilicity.

Having this in mind, we explore the feasibility of using stochastic optimization technique genetic algorithm (GA) in association with DFT to find out the low-lying structures of $(Au_2S)_n$ clusters at $n = 1$–8. Interestingly, the global minimum (GM) structures of $(Au_2S)_n$ clusters are very unique, which are planar at $n = 1$–3, three-dimensional at $n = 4$–8. The formation of these structures are attributed to the high stability of triangular or square faces structural unit (Au_3S_3 or Au_4S_4). Chemical bonding and noncovalent interaction index analysis show that the unique geometric properties of $(Au_2S)_n$ clusters result from Au⋯Au aurophilicity.

Computational methods

A. Structural determination

The low-energy isomers of $(Au_2S)_n$ clusters were located by the combination of GA and DFT method (GA-DFT) implemented in our group, which has been successfully applied in the structural prediction of a number of systems.[34–37] GA is a search heuristic that mimics the process of natural selection.[38–40] This heuristic is routinely used to generate useful solutions to optimization and search problems. The TPSS (Tao, Perdew, Staroverov, and Scuseria)[41] functional was used in DFT calculations, which has been proven reliable in Au–SR clusters,[12,42–44] with the LanL2DZ[45] basis set is used for Au which account for the relativistic effective core potentials of the heavy transition metal, and 6-31G* basis set is used for S atoms. GA cannot promise to find the global minimum structure in one calculation. For each case, five independent GA runs are carried out and the relaxed structures are recorded in one structural bank. Only small basis sets (3-21G for S and Lanl2mb for Au) can be used by global search procedure because of calculation time. The energetic sequences of the isomers may change at larger basis sets, so as many as low-lying isomers in the structural bank are considered. For instance, in optimization of $(Au_2S)_8$, the population size is 20, and the maximum iteration number is 500. After similarity checking of the topological structures, the top 80 lowest energy TPSS/Lanl2MB/3-21G isomers in the structural bank are resorted by the single point energy of high level TPSS/LanL2DZ/6-31G*. Finally, the top 30 lowest energy isomers are fully relaxed at TPSS/LanL2DZ/6-31G* level of theory. The per-atom binding energies (E_b) were calculated based on the optimized structures, which is defined as $E_b = [E(Au_2S)_n - 2n \times E(Au) - n \times E(S)]/n$. Then, vertical electron affinity $VEA = E(Au_2S)_n - E[(Au_2S)_n^-]$, and the vertical ionization potential $VIP = E[(Au_2S)_n]^+ - E(Au_2S)_n$ are calculated under TPSS/LanL2DZ/6-311+G* level of theory. All DFT calculations were performed on the GAUSSIAN 09 package[46] and molecular visualization is performed using MOLEKEL 5.4.

B. Adaptive natural density partitioning (AdNDP) method

Chemical bonding analysis for the located structures was performed using the Adaptive Natural Density Partitioning (AdNDP) method developed by Zubarev and Boldyrev.[47–49] This method was widely used to analysis chemical bonding in molecules and clusters. The algorithm is a generalization of the natural bonding orbital analysis and is based on the diagonalization of the blocks of the first-order density matrix in the basis of natural atomic orbitals. AdNDP analysis are dependent on the choice of the threshold values for the occupation numbers which is inherited from the parental Natural Bond Orbital (NBO) analysis. This method accepts only those bonding elements whose occupation numbers (ON) exceed the specified threshold values, which are usually chosen to be close to 2.00 |e|. AdNDP represents the electronic structure in terms of *n*-center-two-electron (*n*c-2e) bonds with *n* ranging from one to the total number of atoms in the whole molecule. AdNDP recovers both Lewis bonding elements (1c-2e and 2c-2e) and delocalized bonding elements (*n*c-2e), is a very efficient and visual approach to interpretation of the molecular orbital-based wave functions.

C. Noncovalent interaction (NCI) index analysis

The Au⋯Au aurophilic interaction is a kind of weak noncovalent interaction and can be studied by many methods. In this work, the noncovalent interaction (NCI) index method developed by Yang group[50,51] was selected in our analyses, which has been proven reliable in extremely large systems. This method is an approach to detect weak interactions based on the electron density and its derivatives, the analysis results agree with the atoms in molecules approach in characterization of interatomic interactions and it is applicable to extremely large systems and provides a rich representation of van der Waals (VDW) interactions, hydrogen bonds, and steric repulsion. The definition of NCI index is based on the reduced density gradient, s, and the electron density, ρ, where

$$s = \frac{1}{2(3\pi^2)^{1/3}} \frac{|\nabla\rho|}{\rho^{4/3}}$$

and which permits to highlight interactions characterized by a low-density regime. The bonded and nonbonded interactions can then be identified by the sign of the second Hessian eigenvalue (λ_2), whereas the density itself provides information about their strength. The analysis results are shown in scatter plots of the reduced density gradient (s) *versus* the electron density (ρ) multiplied by the sign of λ_2. The low-density regime represents noncovalent/weak interactions. The low-density, low-reduced gradient trough lies at negative values ($\lambda_2 < 0$), indicative of an attractive interaction, and $\lambda_2 > 0$ indicative of a steric repulsion. The low-gradient NCI isosurfaces are colored according to the corresponding values of sign(λ_2)ρ. NCI isosurfaces are a good indicator of interaction strength, where blue represents strong stabilizing interactions and red represents strong unstabilizing interactions. The NCI studies are carried out using Multiwfn package,[52] and the NCI isosurface images are created using VMD.[53]

Results and discussions

A. Geometry structures

Combing the GA with DFT method, we obtained the low-energy isomers for $(Au_2S)_n$ ($n = 1$–8) clusters at the TPSS/

LANL2DZ/6-31G* level. All the isomers are verified to be true local minima by frequency check. Fig. 1 plots the GM and low-energy isomers.

$(Au_2S)_1$. The GM (1A) is a V-shaped configuration with Au–S bond distances of 2.28 Å and Au–S–Au bond angle of 90.7°.

$(Au_2S)_2$. 2A (C_2) is a quasi-planar configuration with Au–S bond distances of 2.31–2.33 Å and Au–S–Au bond angle of 87.4°. 2B is in C_s symmetry, which is higher in energy than 2A by 0.27 eV. 2C is in D_{2d} symmetry and higher than 2A by 0.40 eV in energy. The first three isomers can be seen as two Au_2S molecules attracted by Au···Au interactions. The compact isomer (2D) is 0.87 eV higher in energy than 2A.

$(Au_2S)_3$. The GM (3A) and the second isomer (3B) both have a Au_3S_3 triangular ring, and the remaining three Au are linked to S. The compact isomer (3C) is 0.67 eV higher in energy than 3A.

$(Au_2S)_4$. The GM (4A) has two edge-shared Au_3S_3 triangular rings plus two Au atoms linked to S. Interestingly, there is a remaining Au atom, which is isolated and is not bonded with any S atom. 4B is a Au_6S_4 tetrahedral cage plus two isolated Au atoms and is only 0.06 eV higher in energy. 4C has a distorted Au_4S_4 square ring. 4D and 4E are similar to 4A and 4B, respectively, in geometry. 4F (D_{2d}) has similar bonding model with 3A, which has a Au_4S_4 square ring, but is poor in stability due to lack of Au···Au interaction.

$(Au_2S)_5$. The GM (5A) is a Au_7S_5 cage plus one linked Au atom and two isolated Au atoms, where the cage has two Au_3S_3 triangular faces and one Au_4S_4 square face. 5B is a Au_8S_5 rectangular-pyramid cage (four Au_3S_3 triangular faces and one Au_4S_4 square face) plus two isolated Au atoms, and is only 0.09 eV higher in energy than 5A. 5C is a compact isomer. 5B and 5C both have one four-coordinated sulfur atom.

$(Au_2S)_6$. The GM structure (6A) has a C_{2v} symmetry, which has a triangular prism unit (Au_9S_6). In the triangular prism unit, there are six S in the vertices, nine Au on the edges, and the remaining three isolated Au atoms are located in the central and outside of the triangular prism unit separately. 6B is a compact structure, which has one four-coordinated sulfur atom. 6C and 6D have a close resemblance with 6A, but the location of the three isolated Au is different.

$(Au_2S)_7$. The ground state 7A (C_{2v}) is a $Au_{11}S_7$ cage plus three isolated Au atoms, where the cage has two Au_3S_3 triangular faces and four Au_4S_4 square faces. 7B (C_s) is a $Au_{12}S_7$ cage (four Au_3S_3 faces and two Au_4S_4 faces) plus two isolated Au atoms. 7C (C_s) has one Au_3S_3 ring and three Au_4S_4 rings. 7A has one four-coordinated sulfur atom, and 7B has three four-coordinated sulfur atom.

$(Au_2S)_8$. 8A (S_4) is a $Au_{14}S_8$ cage plus two isolated Au atoms. The cage has four Au_3S_3 triangular faces and four Au_4S_4 square

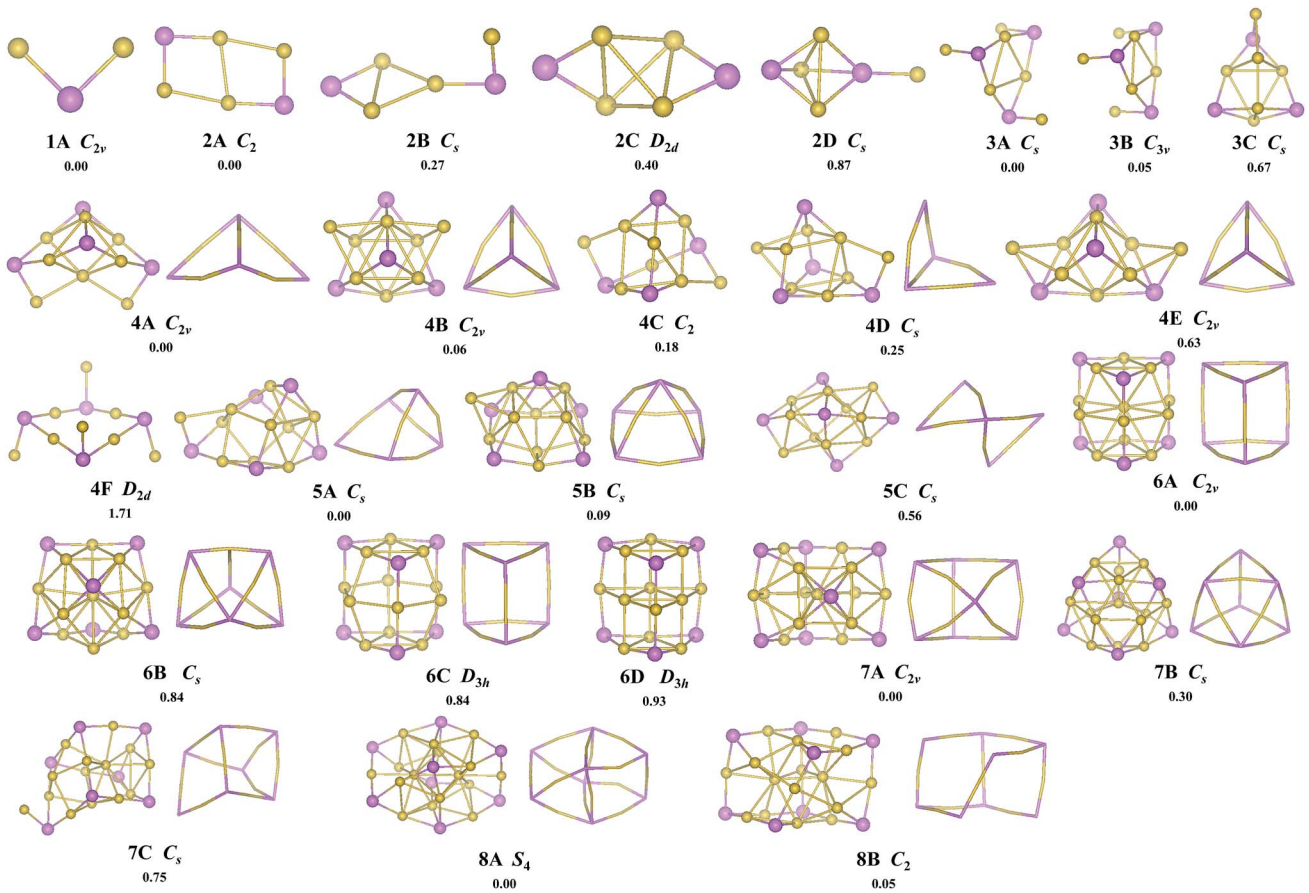

Fig. 1 The global minimum and low-energy isomers and the bonding framework of $(Au_2S)_n$ ($n = 1$–8) clusters at the TPSS/LanL2DZ/6-31G* level. Labelled are the point groups and relative energies in eV. (Au yellow, S purple).

faces. 8A has four four-coordinated sulfur atoms. 8B (C_2) is a $Au_{10}S_8$ cage plus two linked Au atoms and four isolated Au atoms, which is close to 8A in energy (higher than 8A by only 0.05 eV).

In summary, 1A is a V-type Au_2S molecule. 2A is a union of two isolated Au_2S molecules linked by three Au···Au contacts. 3A is a linkage of three Au_2S molecules by three Au–S bonds in a circle manner to form a stable Au_3S_3 triangular ring. 4A has two Au_3S_3 triangular rings plus two linked Au atoms and one isolated Au atom. 5A is a polyhedron (S at the vertices and Au at the edges) plus one linked Au atom and two isolated Au atoms. 6A, 7A and 8A both are polyhedron plus isolated Au atoms. In 7A and 8A, there are four-coordinated sulfur atoms.

B. Electronic stability

Table 1 gives the average binding energies (E_b), energy gaps between the highest occupied molecular orbital and the lowest unoccupied molecular orbital (E_{HL}), vertical electron affinities (VEAs), and vertical ionization potentials (VIPs) of the GMs of $(Au_2S)_n$ (n = 1–8). The fairly large average binding energies (4.89–65.08 eV) and VIPs (7.61–8.25 eV), and relatively small VEAs (1.69–3.46 eV) suggest high electronic stability of these clusters.

The E_{HL} gaps (0.59–1.53 eV) are not so large compared to some other stoichiometric sulfide clusters. Moreover, Au···Au aurophilic contact may decrease the E_{HL} gaps. For example, 2A can be seen as two 1A connected by Au···Au aurophilic interactions, and the E_{HL} gap of 2A (0.80 eV) is much smaller than that of 1A. 4A has the smallest E_{HL} gap (0.59 eV) among all GMs, because it has a open geometry and contains an isolated Au atom attracted by only Au···Au aurophilic interactions.

C. AdNDP chemical bonding analysis

From the geometry, the bonding patterns of the GM structures seem very novel. For examples, 2A is a quasi-planar structure, and it seems to consist of two V-shaped 1A and three Au···Au interactions; there are isolated Au atoms in 4A–8A, which are not bonded with any S atoms. In order to get insight into the chemical bonding of these the clusters, chemical bonding analysis is carried out using AdNDP method.

Fig. 2A plots the AdNDP chemical bonding of 1A, which is very straight forward. The full-filled 5d orbitals of Au (with occupancy number ON = 1.96–2.00 |e|) are not shown in this figure. Excluding Au(5d) orbital, 1A has 8 valence electrons (2 × 1(Au) + 6 × 1(S)), with each gold atom contributing one valence electron and each sulfur atom contributing six valence electrons. Based on AdNDP analysis, four electrons are localized along the two two-center two-electron (2c-2e) Au–S σ-bonds with occupied number ON = 1.99|e|. The remaining 4 electrons are two lone pairs (LPs) with one s-type (ON = 1.97|e|) and one p-type (ON = 1.95|e|) on the sulfur atom.

Fig. 2b plots the AdNDP chemical bonding of 2A. The 8 valence pairs are localized as 4 Au–S σ-bonds (ON = 1.82|e|, 1.92|e|) and 4 LPs in S (ON = 1.91|e|, 1.94|e|). As expected, all the electrons have been assigned in the two Au_2S units, and there is no covalent bonding between the two Au_2S units. In another word, Au···Au aurophilic interaction between the two Au_2S units is a kind of non-Lewis/non-covalent interaction. Such a non-Lewis Au···Au aurophilic interaction is not too weak, which is due to the sd hybridization and d–d interaction in gold and leads to obvious decrease of the ONs of Au–S bonds and E_{HL} gap.

As shown in Fig. 2c, AdNDP chemical bonding of 3A is also very straight forward, which contains 9 Au–S bonds (ON = 1.88–1.95|e|) and 3 LPs of S (ON = 1.96|e|).

There are 16 valence pairs in 4A. As shown in Fig. 2d, AdNDP analysis reveals 4 LPs (ON = 1.93–1.94|e|) of S and 12 Au–S σ-bonds (ON = 1.87–1.90|e|). All the electrons are assigned on

Table 1 The binding energies, E_{HL} gaps, VEAs, and VIPs of the GM structures of $(Au_2S)_n$ (n = 1–8) clusters

	E_b (eV)	E_{HL} (eV)	VEA (eV)	VIP (eV)
1A	−4.89	1.53	1.69	8.25
2A	−5.83	0.80	2.85	7.84
3A	−6.65	1.53	2.54	7.67
4A	−7.04	0.59	3.46	7.63
5A	−7.58	0.89	3.40	7.80
6A	−7.98	1.46	3.13	7.86
7A	−8.04	1.20	3.22	7.61
8A	−8.14	1.41	3.27	7.64

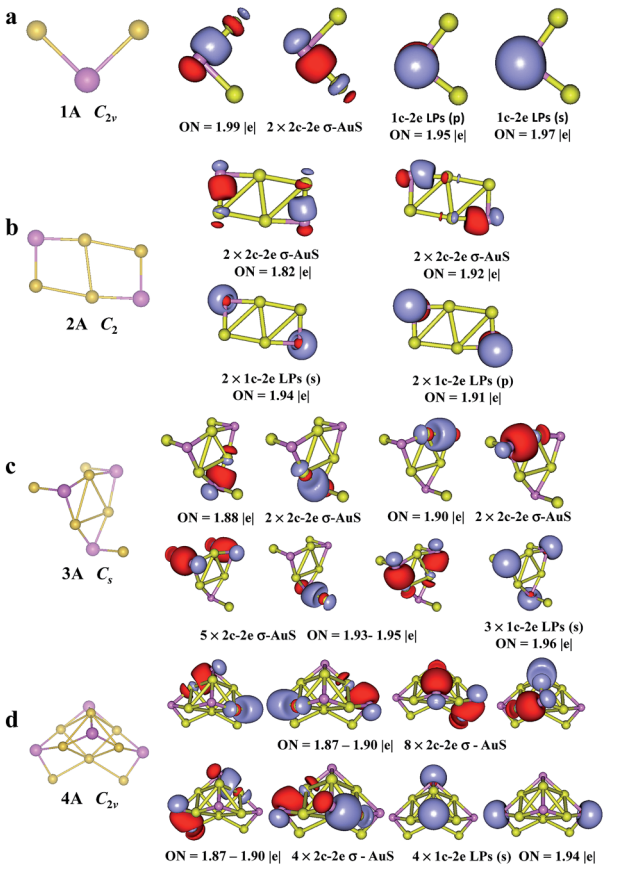

Fig. 2 The results of the AdNDP localization for 1A (a), 2A (b), 3A (c), and 4A (d). Labeled are the occupancy numbers (ONs).

the Au_7S_4 framework, and there is no covalent interaction between the isolated Au and the Au_7S_4 unit. Thus, 4A is more reasonably described in the formulation $[Au_7S_4]^-\cdot Au^+$ based on the electronic structure.

The chemical bonding of some larger clusters (5A, 6C, 7A, and 8A) are also studied using AdNDP method (see Fig. s1 in ESI†). It is found that all these clusters can be viewed as a $[Au_{2n-x}S_n]^{x-}$ anionic unit plus x isolated Au^+ cations. Fig. 3 plots the geometric illustration of $(Au_2S)_n$ (n = 4–8) clusters: $[Au_7S_4]^-\cdot Au^+$ (4A); $[Au_8S_5]^{2-}\cdot 2Au^+$ (5A); $[Au_9S_6]^{3-}\cdot 3Au^+$ (6C); $[Au_{11}S_7]^{3-}\cdot 3Au^+$ (7A); $[Au_{14}S_8]^{2-}\cdot 2Au^+$ (8A). The anionic structural units at n = 4 and 5 have open geometric shells, which leads to relative low E_{HL} gaps (0.59–0.89 eV). On contrary, the anionic structural units have closed geometric shells at n = 6–8, which leads to more stable electronic structures (E_{HL} = 1.20–1.46 eV). The $[Au_{2n-x}S_n]^{x-}$ anionic unit has a closed-shell electronic structure. For example, the $[Au_9S_6]^{3-}$ anionic unit of 6A is a triangular-prism cage, which has a much higher E_{HL} gap (2.76 eV) than 6A (1.46 eV).

D. Electron localization function (ELF) analysis

The chemical bonding structures have been shown clearly by AdNDP chemical bonding analysis. Based on AdNDP analysis, 2A is a union of two 1A by three non-bond Au···Au aurophilic interactions. To verify the results of AdNDP chemical bonding, taking Au_2S (1A) and $(Au_2S)_2$ (2A) as test cases, we performed the electron localization function (ELF) analysis.[54] ELF is a popular method for electronic structures, which is a simple measure of the electron localization in atomic and molecular systems, and its range of values is between 0 (no localization, blue) and 1 (complete localization, red). Geometrical parameters (bond length, in Å, bond angle, in deg) of 1A and 2A (left) and their ELF cut planes (right) are illustrated in Fig. 4. The ELF cut plane of 2A can also been seen as a union of two 1A. The ELF value close to 0.4 corresponds to the Au–S bond, and can be seen as a white color around the Au and S atoms. The cluster–substrate contact shows narrow necks of blue between Au and Au atoms indicating no chemical bonding. This is in agreement with AdNDP chemical bonding analysis, further confirming that there is no covalent bonding between the two Au_2S units. Moreover, from the geometric parameters, 2A can also be viewed as a union of two isolated V-type Au_2S molecules linked by Au···Au contacts.

E. Aurophilic interactions

Based on above geometric and chemical bonding analysis, the Au···Au interactions play an important role in the stability of $(Au_2S)_n$ clusters. Typically, the first three isomers of Au_4S_2 (2A–C) consist of two isolated Au_2S molecules attracted by only Au···Au aurophilic interactions. In all cases the short intramolecular Au–Au distances (<3.1 Å) combined with small Au–S–Au angles (<90.7°) indicate the influence of aurophilic bonding. To have a comparison of the three isomers, the average strength of Au···Au aurophilic interactions is roughly measured: $E_{Au\cdots Au} = [2 \times E(Au_2S) - E(Au_2S)_2]/N_{Au\cdots Au}$, where $N_{Au\cdots Au}$ is the number of Au···Au contacts. As shown in Fig. 5a, the aurophilic interactions in 2A and 2B both are in-plane, but the aurophilic interactions in 2C is 3-dimensional. The average strength of Au···Au interactions ($E_{Au\cdots Au}$) in 2A, 2B, and 2C are 0.64 eV, 0.82 eV, and 0.40 eV, respectively. Interestingly, 2C has the most Au···Au contacts, but its total Au···Au aurophilic interaction is the weakest. Thus, in-plane motifs are favored more by Au···Au aurophilic interactions, which is in good agreement with the planar motifs of small Au clusters.[7] It is well known that the strength of hydrogen bonds is about 0.2 eV. In

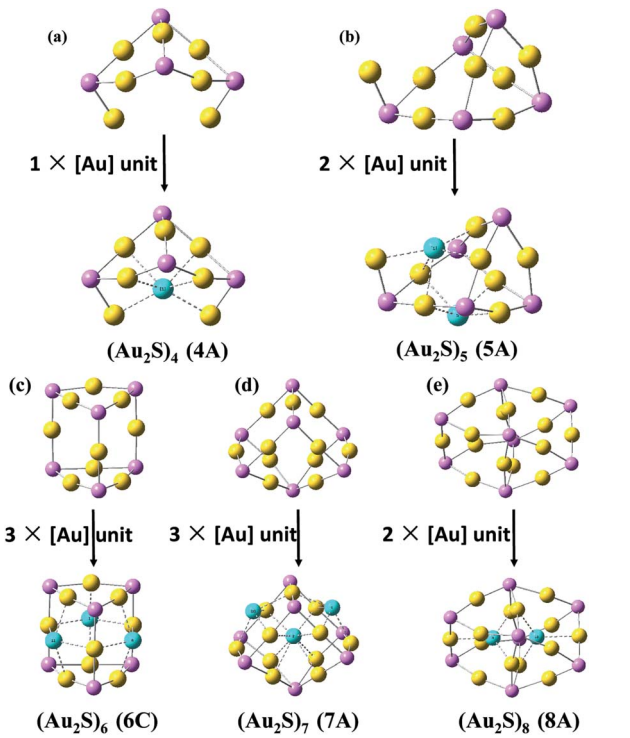

Fig. 3 Frameworks of $(Au_2S)_n$ (n = 4–8) clusters: (a) 4A: $[Au_7S_3]^-\cdot Au^+$; (b) 5A: $[Au_8S_5]^{2-}\cdot 2Au^+$; (c) 6C: $[Au_9S_6]^{3-}\cdot 3Au^+$; (d) 7A: $[Au_{11}S_7]^{3-}\cdot 3Au^+$; (e) 8A: $[Au_{14}S_8]^{2-}\cdot 2Au^+$.

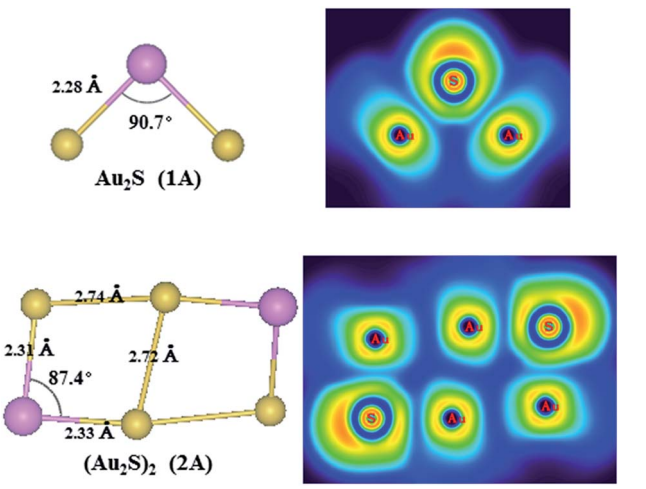

Fig. 4 Geometrical parameters (bond length, in Å, bond angle, in degree) of Au_2S (1A) and $(Au_2S)_2$ (2A) (left) and their ELF cut planes (right).

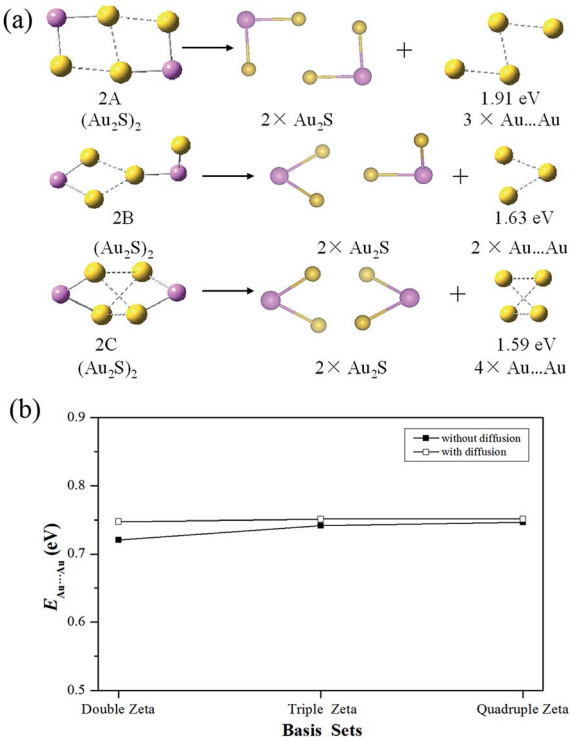

Fig. 5 (a) Comparison of the Au···Au aurophilic interactions in the three isomers (2A, 2B and 2C) of $(Au_2S)_2$ at TPSS/LanL2DZ/6-31G*. (Au yellow, S purple). (b) Average strength of Au···Au interactions in 2A as a function of the size of basis sets using the TPSS functional. Double zeta: cc-pVDZ-pp; triple zeta: cc-pVTZ-pp; quadruple zeta: cc-pVQZ-pp. Diffusion: aug-cc-pV*X*Z-PP.

comparison, such a Au···Au aurophilic interaction is a very strong non-Lewis interaction (0.4–0.8 eV). The calculated $E_{Au\cdots Au}$ in 2A is 0.64 eV with the LanL2DZ basis set. However, the calculated strength of Au···Au aurophilic interactions be influenced by the size of basis sets. Fig. 5b plots the average strength of Au···Au aurophilic interactions in 2A as a function of the size of basis set for Au (double, triple, and quadruple zeta; with and without diffusion). It can be seen that the calculated $E_{Au\cdots Au}$ increases with the size of basis set, and $E_{Au\cdots Au}$ is about 0.75 eV at a very large basis set. However, the increment is not too large, and we chose the smaller LanL2DZ basis set for practical reasons.

The Au···Au aurophilic interaction is a kind of non-Lewis/noncovalent interaction and cannot be investigated directly by the natural bonding orbital methods such as AdNDP. However, NCI method is a good tool for noncovalent interactions. Fig. 6 plots the reduced density gradient (s) *versus* the electron density (ρ) multiplied by the sign of λ_2 of some typical structures 1A, 2A, 4A and 6C. In the date of 1A (Fig. 6a), there is a low-gradient spike lying at about $\mathrm{sign}(\lambda_2)\rho = -0.003$ au, which represents strong stabilizing noncovalent interactions (Au···Au aurophilic interaction). However, there is also a low-gradient spike lying at about $\mathrm{sign}(\lambda_2)\rho = 0.0045$ au, which represents strong unstabilizing interactions. Therefore, the two Au atoms in 1A may be repulsive. As shown in Fig. 6b, there is three strong Au···Au aurophilic interactions ($\mathrm{sign}(\lambda_2)\rho = -0.005$ au) in 2A. However, the two Au atoms in each Au_2S unit are strongly repulsive ($\mathrm{sign}(\lambda_2)\rho = 0.003$ au). The NCI isosurface of 4A and 6C (Fig. 6c and d) reveals two kind of strong weak interactions. The stronger one is the aurophilic interaction between the isolated Au atoms and its neighboring Au atoms ($\mathrm{sign}(\lambda_2)\rho = -0.005$ au). The weaker one is the aurophilic interaction between Au atoms in the Au_3S_3 rings ($\mathrm{sign}(\lambda_2)\rho = -0.003$ au). The isolated Au atom in 4A is attracted by six strong Au···Au aurophilic interactions, and each isolated Au atom in 6C is attracted by four strong Au···Au aurophilic interactions.

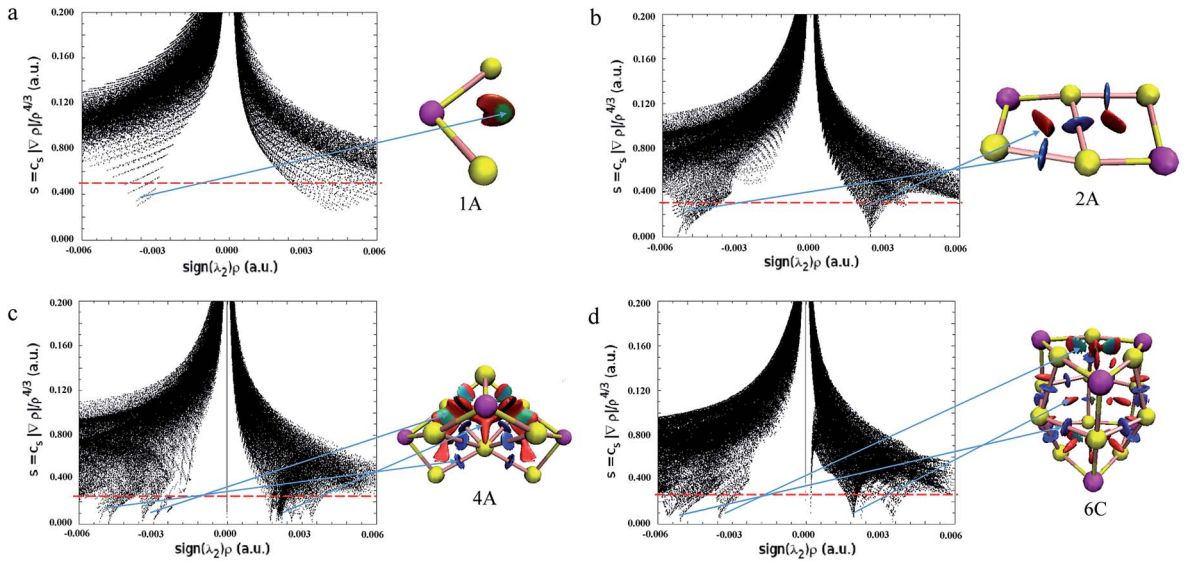

Fig. 6 Plots of the reduced density gradient (s) *versus* the electron density (ρ) multiplied by the sign of λ_2 for (a) 1A, (b) 2A, (c) (4A) and (d) 6C. Inserted are the NCI isosurfaces, which are generated at $s = 0.5$ au, 0.3 au, 0.25 au, and 0.25 au for 1A, 2A, 4A and 6C, respectively. The surfaces are colored on a blue-green-red scale according to values of $\mathrm{sign}(\lambda_2)\rho$, ranging from −0.06 to 0.06 au. Blue indicates strong attractive interactions, and red indicates strong nonbonded overlap.

Conclusion

In summary, the putative GM structures of stoichiometric gold–sulfur clusters $(Au_2S)_n$ (n = 1–8) have been predicted by means of GA, in conjunction with DFT, relying on TPSS functional. The GM of $(Au_2S)_2$ is a union of two isolated V-type Au_2S molecules linked by only Au···Au contacts. The GM of $(Au_2S)_3$ contains a stable Au_3S_3 triangular ring (S at vertices and Au at edges). In the GM of $(Au_2S)_4$, there are two Au_3S_3 triangular rings sharing one edge (AuS_2). At n = 5–8, the GM structures contain $Au_{2n-x}S_n$ polyhedral cage with Au_3S_3 and Au_4S_4 faces. At n = 4 and 5, there are both linked and isolated Au atoms. At n = 6–8, all of the remaining Au atoms are isolated, which are not bonded with any S atom and are filled in the $Au_{2n-x}S_n$ polyhedron by only Au···Au contacts. Direct evidences of the chemical bonding are given AdNDP analysis. AdNDP chemical bonding shows that, at $n \geq 4$, the clusters should be viewed as $[Au_{2n-x}S_n]^{x-} \cdot xAu^+$, where the Au^+ cations are isolated and do not participate any covalent bond. The Au···Au aurophilic interactions play an important role in the stability of $(Au_2S)_n$ clusters, and direct evidence for the Au···Au aurophilicity are given by a noncovalent interaction index analysis.

Acknowledgements

This work is supported by the National Natural Science Foundation of China (Grant Nos 21273008). The calculations are carried out on the High-Performance Computing Centre of Anhui University.

Notes and references

1 P. Pyykko, *Annu. Rev. Phys. Chem.*, 2012, **63**, 45–64.
2 X. Zhou, W. Xu, Y. Wang, Q. Kuang, Y. Shi, L. Zhong and Q. Zhang, *J. Phys. Chem. C*, 2010, **114**, 19607–19613.
3 H. Wei, Z. Wang, L. Yang, S. Tian, C. Hou and Y. Lu, *Analyst*, 2010, **135**, 1406–1410.
4 A. Retnakumari, S. Setua, D. Menon, P. Ravindran, H. Muhammed, T. Pradeep, S. Nair and M. Koyakutty, *Nanotechnology*, 2010, **21**, 055103.
5 S. Saha, A. Pal, S. Kundu, S. Basu and T. Pal, *Langmuir*, 2009, **26**, 2885–2893.
6 P. Pawinrat, O. Mekasuwandumrong and J. Panpranot, *Catal. Commun.*, 2009, **10**, 1380–1385.
7 P. Pyykko, *Chem. Soc. Rev.*, 2008, **37**, 967.
8 L. Wang, J. Bai, A. Lechtken, W. Huang, D. Schooss, M. Kappes, X. Zeng and L. Wang, *Phys. Rev. B: Condens. Matter Mater. Phys.*, 2009, **79**, 033413.
9 W. Huang and L. Wang, *Phys. Rev. Lett.*, 2009, **102**, 153401.
10 B. Assadollahzadeh and P. Schwerdtfeger, *J. Chem. Phys.*, 2009, **131**, 064306.
11 J. Li, X. Li, H. J. Zhai and L. Wang, *Science*, 2003, **299**, 864.
12 D. Jiang, W. Chen, R. Whetten and Z. Chen, *J. Phys. Chem. C*, 2009, **113**, 16983–16987.
13 M. Walter, J. Akola, O. Lopez-Acevedo, P. Jadzinsky, G. Calero, C. Ackerson, R. Whetten, H. Gronbeck and H. Hakkinen, *Proc. Natl. Acad. Sci. U. S. A.*, 2008, **105**, 9157–9162.
14 N. Shao, Y. Pei, Y. Gao and X. Zeng, *J. Phys. Chem. A*, 2008, **113**, 629–632.
15 H. Hakkinen, *Chem. Soc. Rev.*, 2008, **37**, 1847–1859.
16 L. Ren and L. Cheng, *Comput. Theor. Chem.*, 2012, **984**, 142–147.
17 L. Wang, R. Pal, W. Huang, X. Zeng and L. Wang, *J. Chem. Phys.*, 2009, **130**, 051101.
18 M. Zhu, C. M. Aikens, F. J. Hollander, G. C. Schatz and R. Jin, *J. Am. Chem. Soc.*, 2008, **130**, 5883–5885.
19 M. Heaven, A. Dass, P. White, K. Holt and R. Murray, *J. Am. Chem. Soc.*, 2008, **130**, 3754–3755.
20 P. Jadzinsky, G. Calero, C. Ackerson, D. Bushnell and R. Kornberg, *Science*, 2007, **318**, 430–433.
21 L. Cheng, C. Ren, X. Zhang and J. Yang, *Nanoscale*, 2013, **5**, 1475–1478.
22 L. Cheng, Y. Yuan, X. Zhang and J. Yang, *Angew. Chem., Int. Ed.*, 2013, **52**, 9035–9039.
23 H. Qian, W. Eckenhoff, Y. Zhu, T. Pintauer and R. Jin, *J. Am. Chem. Soc.*, 2010, **132**, 8280–8281.
24 Y. Pei, Y. Gao and X. Zeng, *J. Am. Chem. Soc.*, 2008, **130**, 7830–7832.
25 Y. Pei, N. Shao, H. Li, D. Jiang and X. Zeng, *ACS Nano*, 2011, **5**, 1441–1449.
26 A. Bagaturyants, A. Safonov, H. Stoll and H. Werner, *J. Chem. Phys.*, 1998, **109**, 3096.
27 A. Schaefer and R. Ahlrichs, *J. Am. Chem. Soc.*, 1994, **116**, 10686–10692.
28 A. Schafer, C. Huber, J. Gauss and R. Ahlrichs, *Theor. Chim. Acta*, 1993, **87**, 29–40.
29 M. B. Sigman, A. Ghezelbash, T. Hanrath, A. E. Saunders, F. Lee and B. A. Korgel, *J. Am. Chem. Soc.*, 2003, **125**, 16050–16057.
30 W. P. Lim, Z. Zhang, H. Y. Low and W. S. Chin, *Angew. Chem., Int. Ed.*, 2004, **116**, 5803–5807.
31 C. L. Kuo and M. H. Huang, *J. Phys. Chem. C*, 2008, **112**, 11661–11666.
32 F. Scherbaum, A. Grohmann, B. Huber, C. Krüger and H. Schmidbaur, *Angew. Chem., Int. Ed.*, 1988, **27**, 1544–1546.
33 P. Pyykkö and N. Runeberg, *Angew. Chem., Int. Ed.*, 2002, **114**, 2278–2280.
34 R. Li and L. Cheng, *Comput. Theor. Chem.*, 2012, **996**, 125–131.
35 Y. Yuan and L. Cheng, *Int. J. Quantum Chem.*, 2012, **113**, 1264–1271.
36 L. Ren, L. Cheng, Y. Feng and X. Wang, *J. Chem. Phys.*, 2012, **137**, 014309.
37 L. Cheng, *J. Chem. Phys.*, 2012, **136**, 104301.
38 D. M. Deaven and K. M. Ho, *Phys. Rev. Lett.*, 1995, **75**, 288–291.
39 R. L. Johnston, *Dalton Trans.*, 2003, 4193–4207.
40 A. Shayeghi, D. Götz, J. Davis, R. Schaefer and R. L. Johnston, *Phys. Chem. Chem. Phys.*, 2015, **17**, 2104–2112.
41 T. Jianmin, J. P. Perdew, V. N. Staroverov and G. E. Scuseria, *Phys. Rev. Lett.*, 2003, **91**, 146401.

42 A. Lechtken, C. Neiss, M. M. Kappes and D. Schooss, *Phys. Chem. Chem. Phys.*, 2009, **11**, 4344–4350.
43 M. Johansson, A. Lechtken, D. Schooss, M. Kappes and F. Furche, *Phys. Rev. A*, 2008, **77**, 053202.
44 N. Shao, W. Huang, Y. Gao, L. Wang, X. Li, L. Wang and X. Zeng, *J. Am. Chem. Soc.*, 2010, **132**, 6596–6605.
45 P. J. Hay and W. R. Wadt, *J. Chem. Phys.*, 1985, **82**, 299–310.
46 M. Frisch, G. Trucks, H. Schlegel, *et al.*, *Gaussian 09, Revision B.01*, Gaussian, Inc., Wallingford, CT, 2009.
47 D. Zubarev and A. Boldyrev, *Phys. Chem. Chem. Phys.*, 2008, **10**, 5207–5217.
48 D. Zubarev and A. Boldyrev, *J. Phys. Chem. A*, 2008, **113**, 866–868.
49 D. Zubarev and A. Boldyrev, *J. Org. Chem.*, 2008, **73**, 9251–9258.
50 E. Johnson, S. Keinan, P. Mori–Sanchez, J. Contreras–Garcia, A. Cohen and W. Yang, *J. Am. Chem. Soc.*, 2010, **132**, 6498–6506.
51 J. Contreras–Garcia, E. Johnson, S. Keinan, R. Chaudret, J. Piquemal, D. Beratan and W. Yang, *J. Chem. Theory Comput.*, 2011, **7**, 625–632.
52 T. Lu and F. Chen, *J. Comput. Chem.*, 2012, **33**, 580–592.
53 W. Humphrey, A. Dalke and K. Schulten, *J. Mol. Graphics*, 1996, **14**, 33–38.
54 A. Savin, R. Nesper, S. Wengert and T. F. Fassler, *Angew. Chem., Int. Ed.*, 1997, **36**, 1808–1832.